Anatomical Design and Production of a Novel 3-Dimensional Co-Culture System Replicating the Human Flexor Digitorum Profundus Enthesis

Received: 29 November 2023 | Revised: 27 January 2024 | Accepted: 5 February 2024

DOI: 10.1111/joa.14027

Journal of Anatomy | ANATOMICAL SOCIETY WILEY

ORIGINAL ARTICLE

Anatomical design and production of a novel three-dimensional co-culture system replicating the human flexor digitorum profundus enthesis

Jeremy W. Mortimer[1,2] | Philippa A. Rust[1,3] | Jennifer Z. Paxton[1]

[1]Anatomy@Edinburgh, Deanery of Biomedical Sciences, Old Medical School, University of Edinburgh, Edinburgh, UK

[2]School of Anatomy, University of Bristol, Bristol, UK

[3]Hooper Hand Unit, St. John's Hospital, Livingston, Edinburgh, UK

Correspondence
Jennifer Z. Paxton, Anatomy@Edinburgh, Deanery of Biomedical Sciences, Old Medical School, University of Edinburgh, Teviot Place, Edinburgh EH8 9AG, UK.
Email: j.z.paxton@ed.ac.uk

Funding information
Orthopaedic Research UK, Grant/Award Number: 528; The Rooney Plastic Surgery and Reconstructive Surgery Trust

Abstract

The enthesis, the specialized junction between tendon and bone, is a common site of injury. Although notoriously difficult to repair, advances in interfacial tissue engineering techniques are being developed for restorative function. Most notably are 3D in vitro co-culture models, built to recreate the complex heterogeneity of the native enthesis. While cell and matrix properties are often considered, there has been little attention given to native enthesis anatomical morphometrics and replicating these to enhance clinical relevance. This study focuses on the flexor digitorum profundus (FDP) tendon enthesis and, by combining anatomical morphometrics with computer-aided design, demonstrates the design and construction of an accurate and scalable model of the FDP enthesis. Bespoke 3D-printed mould inserts were fabricated based on the size, shape and insertion angle of the FDP enthesis. Then, silicone culture moulds were created, enabling the production of bespoke anatomical culture zones for an in vitro FDP enthesis model. The validity of the model has been confirmed using brushite cement scaffolds seeded with osteoblasts (bone) and fibrin hydrogel scaffolds seeded with fibroblasts (tendon) in individual studies with cells from either human or rat origin. This novel approach allows a bespoke anatomical design for enthesis repair and should be applied to future studies in this area.

KEYWORDS
3D culture, 3D printing, co-culture, enthesis, flexor digitorum profundus, flexor tendon, interfacial tissue engineering

1 | INTRODUCTION

The enthesis is the specialized microanatomical area at the interface where soft tissue (i.e., tendon, ligament, joint capsule) attaches to hard tissue (i.e., bone). It allows uniform force transmission between mechanically distinct tissues through adaptations to counteract the high-stress concentrations, such as an expanded, flared insertion shape (Benjamin et al., 2006; Schlecht, 2012; Shaw & Benjamin, 2007) and a highly irregular interdigitation at the true soft-hard interface (Milz et al., 2002; Shaw & Benjamin, 2007). Most entheses also exhibit an intervening layer of fibrocartilage that provides a transitional zone of increasing stiffness through a gradation of cellular and extracellular matrix (ECM) properties (Apostolakos et al., 2014; Doschak & Zernicke, 2005), diminishing

compression and shear forces generated by changes in the angle of inserting fibres (Benjamin et al., 1991; Benjamin & Ralphs, 1998; Evans et al., 1990). Injury to the enthesis heals poorly, as these specialized features listed above are not well restored even with surgical repair, producing a generalized fibrovascular scar with sub-physiological biomechanical properties (Galatz et al., 2006; Liu et al., 1997; Rodeo et al., 1993; Silva et al., 2006; Thomopoulos et al., 2003).

Interfacial tissue engineering (ITE) provides the opportunity to study and generate the enthesis in vitro, ultimately aiming to provide a pre-formed soft-hard tissue interface for surgical replacement as an improved therapeutic option. However, ITE enthesis models lack clinical applicability particularly due to a disregard of anatomical (micro-)structure and proportion. Although the cellular, biochemical and biomechanical components are well considered (Boys et al., 2017; Calejo et al., 2019; Font Tellado et al., 2015; Lei et al., 2021; Moffat et al., 2009; Patel et al., 2018; Paxton, Baar, & Grover, 2012; Shiroud Heidari et al., 2021; Smith et al., 2012; Yang & Temenoff, 2009), the inclusion of anatomical information, such as morphometric analysis of the particular region, would hasten the 'bench to bedside' transition (Loukopoulou et al., 2022). Incorporating dimensional aspects such as scale, sizing, shape and angle requires an innovative approach to manipulating the cell culture environment, and the main purpose of this study is to address this demand by creating novel, bespoke, culture-well geometry. Importantly, this methodological concept is applicable and relevant to ITE of distinct anatomical regions, as properties critical for anatomical design in one area are unlikely to be appropriate for another interfacial region (Loukopoulou et al., 2022).

A key approach to ITE is co-culture of different cell types. Heterogenous cell–cell contact and communication improves the in vivo simulation of multicellular tissue models (Goers et al., 2014), with paracrine signalling between cell populations influencing cell response, function, and gene expression (Bicho et al., 2018). In 2-dimensional (2D) enthesis co-culture, the potential for cellular transdifferentiation and eventual fibrocartilage tissue formation has been demonstrated by the expression of fibrocartilage markers at the interface between fibroblast and osteoblast populations (Wang et al., 2007). However, co-culture models must focus on the three-dimensional (3D) environment as a more physiological representation, in which cells demonstrate more natural morphology, cell–cell and cell–environment interactions, improving their viability, proliferation, differentiation, migration, and response to stimuli (Antoni et al., 2015). Such 3D models are, therefore, most appropriate to study cellular interactions as well as to accomplish tissue (re)generation, as a key aim of enthesis ITE development. 3D models inherently require the additional consideration of dimensional design, and, rather than neglect this as a minor feature, we highlight it as an opportunity to greatly enhance clinical applicability.

An example of enthesis injury in the finger is demonstrated by avulsion of the flexor digitorum profundus (FDP) tendon from the distal phalanx (DP) bone, causatively known as 'jersey finger', a common hyperextension injury of the finger mainly associated with sporting trauma (Abergo & Shamrock, 2022; Bachoura et al., 2017; Leddy & Packer, 1977; Ruchelsman et al., 2011; Shapiro & Kamal, 2020; Tuttle et al., 2006). Successful treatment is crucial owing to the high costs of healthcare and loss of productivity from such functionally important hand injuries (de Putter et al., 2012); however, current FDP avulsion repair techniques are suboptimal due to surgical complications (Huq et al., 2013) and low healing strength from lack of functional enthesis regeneration (Silva et al., 2002, 2006) leading to unsatisfactory patient outcomes (Moiemen & Elliot, 2000; Tempelaere et al., 2017; Zhang et al., 2014). Although overlooked as the focus of ITE studies compared to larger joint enthesis injuries [e.g., rotator cuff (shoulder), cruciate ligaments (knee), Achilles tendon (ankle)], the compact size, practicable scale, and relative surgical accessibility of the FDP enthesis make it a convenient early candidate to design and develop an anatomically sized tissue-engineered replica, with potentially less complex future surgical implantation. Accordingly, we have previously analysed critical morphometric aspects of the FDP enthesis through human cadaveric dissection and histology for this purpose, specifically the size and shape of the tendon insertion footprint on the DP and the angle of inserting tendon fibres (Mortimer et al., 2021). This now requires the translation of the anatomical morphometrics into an ITE culture system that can generate a 3D tendon–bone co-culture construct with the defined enthesis dimensions.

The aim of the study was to design and demonstrate the fabrication of a novel 3D soft-hard tissue co-culture system, and determine the feasibility of integrating real morphometric data and potential for size scaling into the production of anatomically- and clinically relevant ITE models. This was achieved through careful design and creation of bespoke 3D anatomical culture zones based on 2 critical morphometric considerations: (1) the size and shape of the FDP enthesis (Mortimer et al., 2021) and (2) the angle of tendon fibre insertion (Mortimer et al., 2021). These design elements were incorporated into a previously established bone-to-bone ligament model comprised of fibrin hydrogel (soft tissue element) and brushite (hard tissue element) cell scaffolds (Paxton, Grover, & Baar, 2010). The novel model system was then employed to produce human FDP-DP tendon–bone co-culture constructs of average adult dimensions and further clinically relevant sizes.

2 | MATERIALS AND METHODS

2.1 | Isolation and culture of human fibroblasts and osteoblasts

Primary cell cultures of both human tendon fibroblasts (HTFs) and osteoblasts (HObs) were isolated based on an explant protocol (Bakker & Klein-Nulend, 2012) and obtained from surgical discard tissue following informed consent from patients undergoing hand and wrist procedures, at St. John's Hospital, NHS, Edinburgh, UK

(under Tissue Governance approval, BioResource, local ethics committee). Discard digital extensor tendon (for HTFs) and ulna head bone (for HObs) were transported in 5% antibiotic–antimycotic solution (Gibco, Fisher Scientific, Cramlington, UK) in phosphate-buffered saline (PBS) and laboratory-processed under sterile conditions within 2 h.

Tendon tissue was cleared of residual connective tissue under ×3 magnification, minced into small chunks or strands, and copiously washed with PBS. Approximately 10 tissue pieces were each placed into 100 mm diameter dishes, and maintenance culture medium [Dulbecco's modified Eagles medium (DMEM) (Sigma-Aldrich, Gillingham, UK), supplemented with 10% fetal bovine serum (FBS) (Labtech, Heathfield, UK), 2% L-glutamine (Gibco), 2.4% 4-2(2-hydroxyethyl)-1-piperazineethanesulfonic acid (HEPES) buffer (Gibco) and 1% penicillin/streptomycin (Gibco) (S-DMEM)] carefully added (avoiding tissue flotation). The cultures were left undisturbed for 7 days at 37°C, 5% CO_2, to allow outgrow and anchorage of HTFs before the first medium exchange. Standard culture in S-DMEM then continued with the tendon tissue removed and discarded at 1st passage, and the cells used in passages 2 and 3.

Bone samples were meticulously cleaned of connective and hematopoietic tissue, cut into 1–2 mm^2 pieces, thoroughly washed in PBS, and placed into 0.2% collagenase type II solution (Gibco) in DMEM in a 37°C water bath for 2 h with regular vigorous manual shaking, to ensure soft tissue removal. Collagenase deactivation was achieved by repeatedly rinsing and shaking the extracted bone pieces in complete medium [S-DMEM + 25 μM ascorbic acid (AA) (Sigma-Aldrich)], then 10–15 pieces were each placed into 100 mm dishes for HOb explant culture. The initial, continued, and subculture of HObs subsequently proceeded as per HTFs, except with maintenance in complete medium, and the cells were used between passages 2–4.

2.2 | Isolation and culture of rat fibroblasts and osteoblasts

Primary cell cultures of rat tendon fibroblasts (RTFs) were isolated by a collagenase digestion method described previously (Paxton et al., 2009), from euthanized adult Sprague–Dawley rats obtained from local animal facilities at The University of Edinburgh. Bilateral Achilles tendons were dissected out, cleaned of residual connective tissue, and washed with copious PBS under aseptic conditions with ×3 magnification. Tendons were digested in a 0.1% collagenase type II solution in DMEM, incubated at 37°C, 5% CO_2 for 15 h, following which the solution was passed through a 100 μm cell strainer (Falcon, Fisher Scientific) and centrifuged at 1250 rpm for 5 min. The resulting cell pellet was re-suspended in FBS for collagenase deactivation, then the suspension similarly spun for 2 min, with the final cell pellet re-suspended in S-DMEM. Routine cell culture in S-DMEM continued at 37°C, 5% CO_2, with RTFs used for experiments between passages 2–5.

Rat osteoblasts (RObs) were acquired from Cell Applications, Inc (San Diego, CA, USA) as primary cells from healthy adult rat bone. RObs were cultured routinely in S-DMEM at 37°C, 5% CO_2, and used between passages 10–12.

2.3 | Functional fibroblast and osteoblast characterizations

HTFs and RTFs were tested for their ability to contract a fibrin hydrogel scaffold between 2 suture anchors in the formation of a basic tendon analogue construct, compared to acellular control. The base of 35 mm diameter wells in 6-well plates were coated with 1.5 mL silicone (poly(dimetholsiloxane); PDMS, [Sylgard 184 silicone elastomer Dow Corning, Wiesbaden, Germany]) and left to polymerize in a 50°C oven overnight. 2 × 5.0 mm lengths of number 1 silk suture (Ethicon, Bridgewater, USA) were set down flat onto the PDMS 12 mm apart, end to end in series, held in place by Austerlitz minutiens stainless steel insect pins (Fine Science Tools, Cambridge, UK) at the suture ends. The wells, plate and lid were sterilized by 30 min soaking in 70% ethanol and air-dried before use. Fibrin gels were manufactured based on protocols described elsewhere (Paxton et al., 2009, Paxton et al., 2012; Paxton, Grover, & Baar, 2010). Briefly, 500 μL of 'thrombin mix' [50 μL/mL bovine thrombin (200 U/mL) (Merck, Darmstadt, Germany), 2 μL/mL aminohexanoic acid (200 mM) (Sigma-Aldrich) and 2 μL/mL aprotinin (10 mg/mL) (Sigma-Aldrich)] was added dropwise to cover the entire PDMS-coated well base, then 200 μL of bovine fibrinogen (20 mg/mL) (Sigma-Aldrich) was subsequently added dropwise and the gel left to polymerize at 37°C for 1 h. HTFs or RTFs were seeded onto the fibrin gel in droplets at a density of 100,000 cells in 1 mL S-DMEM/well, whilst acellular controls were left unseeded in 1 mL S-DMEM ($n = 3$ each group). Plates were then incubated at 37°C, 5% CO_2, with 2 mL S-DMEM exchanged every 2–3 days, and regular overview photography was conducted to observe contraction up to day 28.

HObs and RObs were tested for their ability to produce a mineralized ECM in an osteoblast mineralizing medium, compared to controls in their maintenance medium. HObs were seeded in duplicate (per media group) at 100,000 cells per 35 mm well in 2 mL complete medium and incubated at 37°C, 5% CO_2. On day 4 (confluence), complete medium was exchanged for a laboratory-made human osteoblast mineralizing medium (HODM) [S-DMEM + 50 μg/mL AA + 10 nM dexamethasone (Hello Bio, Bristol, UK) + 10 mM β-glycerophosphate (Sigma-Aldrich)], with continued culture in this medium for the test group, whilst the control group continued in complete medium. RObs were similarly set up and cultured, seeding at 50,000 cells in S-DMEM, with media in the test group exchanged for rat osteoblast differentiation medium (RODM), acquired from Cell Applications, Inc (San Diego, CA, USA) and stated to allow mineralization of osteoblast ECM, on day 1, whilst the control group continued in S-DMEM. Cells were fixed with 4% formaldehyde

(Sigma-Aldrich) and stained with alizarin red (Millipore, Merck Life Science, Gillingham, UK) on days 11, 18 and 25, with digital microscope and overview images captured directly after staining.

2.4 | Histological analysis

Basic tendon analogue constructs manufactured from RTFs were fixed in 4% formaldehyde for 1 h at 4°C, before being washed in PBS at 4°C. Samples then underwent standard paraffin wax processing via a Tissue Tek processor and were embedded in wax. Sections of 8 μm were produced in both the transverse and coronal planes, before being stained in Haematoxylin and Eosin for a general overview of tendon analogue structure and Masson's trichrome stain for qualitative collagen assessment.

2.5 | Three-dimensional co-culture system preparation

2.5.1 | Bone anchor

Bone anchors were fabricated from brushite and cast into a specific trapezoidal shape to mimic the FDP bony insertion by a process of reverse moulding, modified from previous work described elsewhere (Paxton, Grover, & Baar, 2010; Figure 1). The intended trapezoidal shape of the bone anchor was first composed and integrated into a multi-shape casting tray as a computer-aided design (CAD) file in Tinkercad software (Autodesk, San Rafael, CA, USA) (Figure 1a). The height, base width and apex width dimensions were determined by previously established measurements of the human FDP insertion trapezoid (Mortimer et al., 2021) whether a 'universal' average size, or a 3-level 'large', 'medium' or 'small' size (Mortimer et al., 2021), with a fixed depth of 2 mm (Table 1). The casting tray was 3D printed in Acrylonitrile Butadiene Styrene (ABS) (Figure 1b), using a ThermoJet solid object printer (3D Systems, Valencia, USA), and an impression mould was created using Kemsil silicone (Associated Dental Products, Swindon, UK) (Figure 1c). Brushite cement was formed by mixing β-tricalcium phosphate powder (β-TCP) (Plasma Biotal, Buxton, UK) with a solution of 3.5 M 85% pure orthophosphoric acid (OA) (Sigma-Aldrich), containing 200 mM citric acid (Sigma-Aldrich) and 200 mM sodium pyrophosphate (Sigma-Aldrich) as retardants, at a powder-liquid ratio of 3.5 g/mL, on a vibrating plate. The cement was immediately packed into the negative shapes of the mould, setting within 30–60 s at room temperature, then the cast bone anchors were removed for sterilization by soaking in 70% ethanol for 30 min and air drying, and subsequently stored for experimental use (Figure 1d).

2.5.2 | Mold insert design

A mould insert was designed in Tinkercad software (Figure 2) to convert a standard 35 mm diameter well into a precise 3D culture

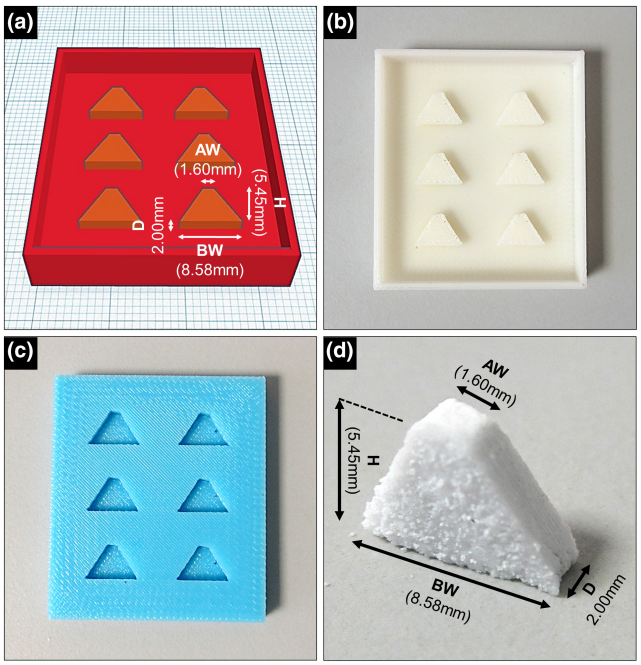

FIGURE 1 Bone anchor production. The 'universal' size is demonstrated, with specific 'universal' size dimensions in parentheses; AW, apex width; BW, base width; D, depth; H, height. (a) Computer-aided design (CAD) of a 6-shape negative impression moulding tray. (b) Three-dimensional (3D) printed tray from (a) in Acrylonitrile Butadiene Styrene (ABS). (c) Kemsil silicone impression mould from (b). (d) Cast brushite bone anchor formed from a single trapezoidal shape impression from (c).

zone, once 3D printed in ABS and surrounded by moulding material. The mould insert design components consisted of a well insert (Figure 2a) and a lattice frame to incorporate 6 well inserts within a single mould for a 6-well plate (Figure 2b).

The 3 key elements of the well insert were:

- an area to position and securely house the bone anchor ('tail');
- an area for tendon analogue formation by hydrogel contraction and culture media containment/exchange ('body');
- a defined angle between the bone anchor area ('tail') and tendon analogue area ('body') matching tendon fibre bony insertion angle.

The size of the 'tail' varied to match the size of the bone anchor (Table 1), and hence determined the overall size of the desired model for the co-culture system—'universal' (average), 'large', 'medium' or 'small'—as per previous anatomical measurements (Mortimer et al., 2021). The angle between the 'tail' and the 'body' was fixed at 30°, similarly based on previous human anatomical analysis of the angle of FDP tendon fibres inserting onto bone (Mortimer et al., 2021). The bone anchor was presented angled from below to allow a horizontal culture surface for tendon analogue formation. The dimensions of the well insert are described in Figure 2a.

The lattice frame component consisted of vertical, horizontal and diagonal struts to suspend 6 well inserts centrally within each

TABLE 1 Bone anchor dimensions with cell seeding number for different model sizes.

Model size	Bone anchor dimensions (mm)				Osteoblast seeding number (cell number/µl S-DMEM)
	Height	Base width	Apex width	Depth	
Universal	5.45	8.58	1.60	2.00	15,000/50
Large	6.36	9.30	1.66	2.00	21,000/42
Medium	5.05	8.30	1.56	2.00	15,000/30
Small	4.33	7.57	1.65	2.00	12,000/24

Note: Dimensions and size categorizations previously determined by Mortimer et al. (2021).

Abbreviation: S-DMEM, supplemented Dulbecco's modified Eagles medium.

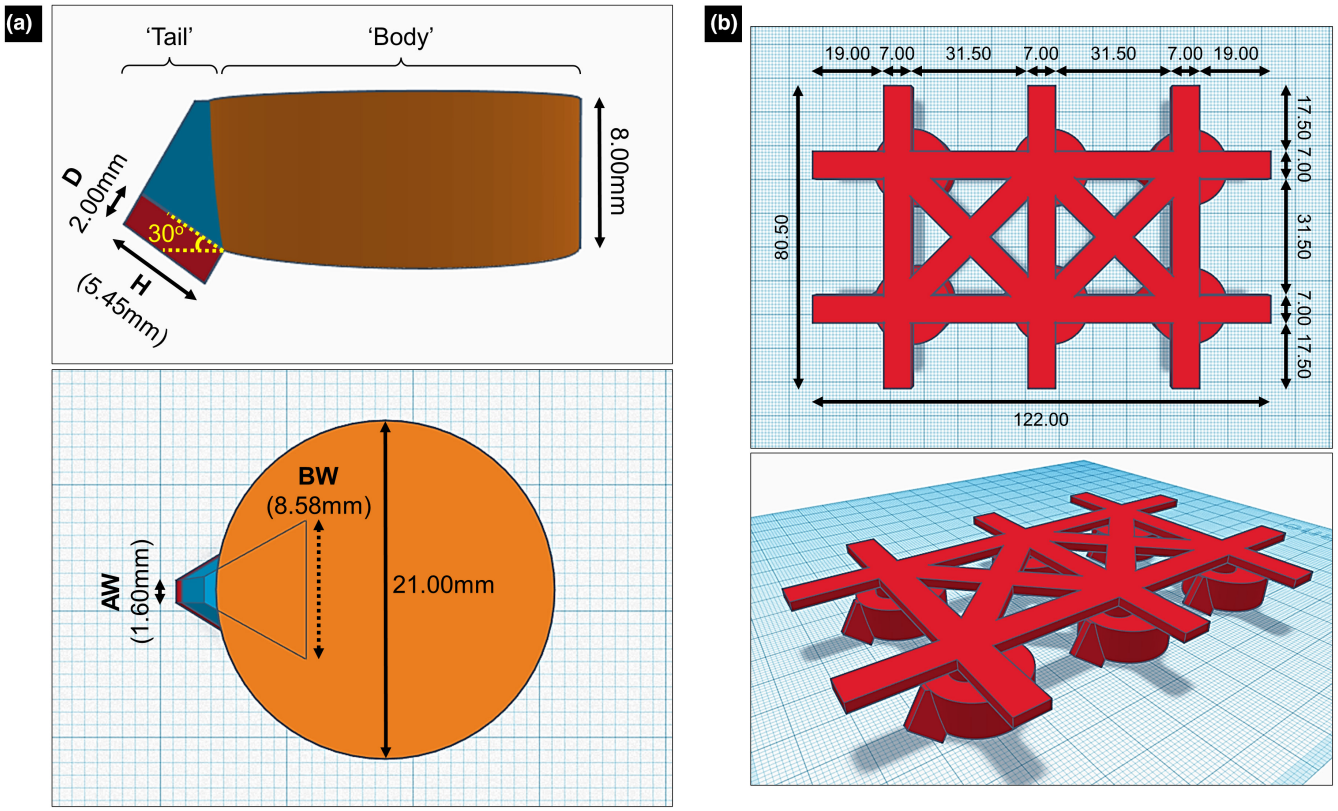

FIGURE 2 Mold insert CAD specifications. The 'universal' size is demonstrated, with specific 'universal' size dimensions in parentheses. (a) Well insert, lateral (*upper panel*) and superior view (*lower panel*). The 'tail', composed of *blue* and *red blocks*, provides space for insertion and housing, respectively, of the bone anchor. The 'body', composed of a cylindrical *brown/orange block*, provides space for the developing tendon analogue. The *red block* mimics the trapezoidal bone anchor size and shape, set at 30° to the horizontal inferior surface of the *brown/orange block*, positioned at the point where its 2 forward-facing bottom corners both intersect the curved edge of the *brown/orange block*. Note the superior and inferior surfaces of the *brown/orange* block are flat but appear rounded in 3D image projection. *H*, *BW* and *AW* of the *red block* (bone anchor) are specific to model size, whilst *D* is common to all sizes (Table 1). The *blue block* continues the 3D shape of the *red block* to the level of the superior surface of the *brown/orange block* to create the space necessary to insert the bone anchor. The dimensions of the *brown/orange* block are common; the 8.00 mm depth was designed large enough to contain a volume of contracting fibrin gel and culture medium without extending above the height of a standard 35 mm diameter well, whilst the 21.00 mm diameter provides the new ample culture space for the tendon analogue, fitting comfortably within a 35 mm diameter well, whilst still allowing enough space for the additional 'tail' components of all specific model sizes. (b) Lattice frame, superior (*upper panel*) and superior oblique view (*lower panel*). All units in millimetres. Frame dimensions were calculated to allow 6 well inserts to each be held centrally within the wells, whatever the model size (well insert) required. Well inserts are suspended centrally by 7.00 mm (diameter) × 4.00 mm (depth) cylinders at the intersection of the horizontal and vertical bars of the lattice. Lattice frame depth 2.00 mm.

of the wells of a standard 6-well plate, whilst allowing a single mould structure to sit unsupported on a lidless plate and providing strength to the overall unit. The dimensions of the lattice frame are described in Figure 2b.

2.5.3 | Component integration and set up

The mould insert was placed on a 6-well plate (Figure 3a), with the well inserts located in the wells away from the well rim (Figure 3b). PDMS was then filled around the well inserts to the level of the superior surface of the 'body' (Figure 3b), requiring approximately 9 mL for each well, and cured in a 50°C oven overnight. For positional security the frame was temporarily fixed to the plate with adhesive tape during PDMS filling and curing. The entire mould insert was then removed to leave the impression of the well insert (Figure 3c).

The suture anchor was prepared by cutting number 1 silk suture with sharp dissecting scissors to the same width as the ideal tendon width of a particular culture model size, ranging from 3.7 to 5.4 mm, based on previously determined width measurements of the human distal FDP tendon 12 mm from bony insertion (Mortimer et al., 2021). The suture was secured flat onto the PDMS with stainless steel insect pins at the suture ends, vertical, parallel and central to the point where the well insert 'body' impression becomes the 'tail' (i.e., the nearest bone anchor edge when in position), at a 12 mm distance (Figure 3d–f). Suture and construct distances were judged under guidance of a millimetre slide rule and ×3 magnification. Plates and lids were then sterilized with 70% ethanol soaking for 30 min, air-dried and stored sterile

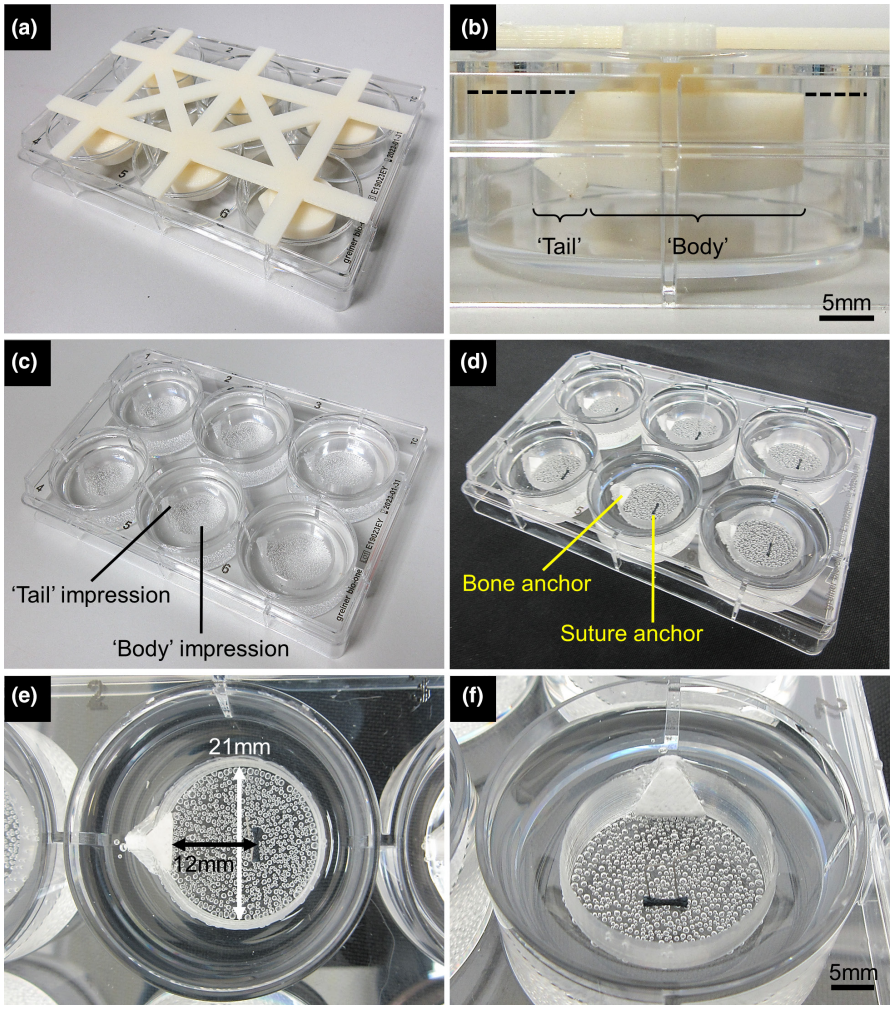

FIGURE 3 Co-culture system set up. 'Universal' size shown. (a) Mold insert in place on a standard lidless 35 mm well diameter 6-well plate. (b) Magnified side view of a single well of the 6-well plate, showing the well insert suspended centrally above the well base. Sylgard is then filled around the well insert up to the broken line. (c) Negative shape impressions of the well inserts produced in the cured Sylgard after removal of the entire mould insert, creating the 3D internal culture zones. (d) Sterilized wells set up with bone anchors and pinned sutures in position. (e) Superior view of a single 35 mm well, displaying the newly created internal culture zone with 21 mm diameter 'body'. The bone anchor is located at the base of the 'tail' of the culture zone, with the suture anchor secured at a 12 mm distance within the 'body'. (f) Superior oblique view of (e), showing the full presenting surface of the bone anchor, ready for addition of the tendon analogue culture components.

before use. A sterile bone anchor, once seeded with osteoblasts, was then positioned into the base of the 'tail' impression (Figure 3d–f) when co-culture was ready to commence.

2.6 | Tendon–bone co-cultures

2.6.1 | 'Universal' human model system

Co-cultures of a 'universal' (average adult) size model system using human cells were prepared in a 6-well plate as described above. Sterile 'universal' bone anchors underwent 6×10 min washes in 1 mL S-DMEM, replenished after each wash, for acid washout and pre-soaking in culture medium. After 30–60 min air drying, HObs were seeded onto the bone anchors (Table 1) by droplet seeding in non-tissue culture-treated plates (Falcon, Fisher Scientific), and incubated for 4–5 h at 37°C, 5% CO_2 for cell attachment. Seeded bone anchors were then moved to a fresh well and cultured in 1 mL HODM for 7 days, with media replacement every 2–3 days, before placing in the base of the 'tail' impression of the culture zone. 1000 μL of thrombin mix was then added dropwise into the 'body impression' of the culture zone, ensuring the whole of the angled bone anchor presenting surface was covered, similarly followed by 400 μL fibrinogen. After 1 h of polymerization at 37°C, HTFs were seeded onto the fibrin gel at a density of 200,000 cells in 1 mL S-DMEM/well ($n=3$) and cultured at 37°C, 5% CO_2, with culture medium changing to a 50:50 mix of S-DMEM:HODM on day 1. Routine culture continued for 28 days with medium change every 2–3 days and overview photography obtained weekly.

2.6.2 | Multi-size model systems

6-well plates of 'large', 'medium' and 'small' culture system model sizes, and bone anchors of corresponding sizes (Table 1), were similarly established, cultured and observed as described for the 'universal' size system ($n=3$ co-culture constructs per model size). RObs were seeded onto each size of bone anchor as per Table 1. The seeded bone anchors were cultured in RODM before integration into the culture system, whilst RTFs were seeded onto the fibrin gel in S-DMEM as per HTFs, with culture medium then changing to a 50:50 mix of S-DMEM:RODM onwards from day 1.

3 | RESULTS

3.1 | Functional fibroblast and osteoblast characterizations

Both HTFs and RTFs were able to similarly contract the fibrin hydrogel around and between suture anchor points to form a basic tendon analogue, indicating required functionality (Figure 4a). The vast proportion of contraction occurred over the first week; within the first few days the fibroblast-seeded gel rapidly contracted from the well rim towards the anchors, and by 7 days the shape of the gel in overview had roughly conformed to the anchor positions, stretched between them. From day 7–14, the gel condensed down further between the anchors, becoming slimmer and denser. Between day 14–28 macroscopic changes were minimal, although a subtle progression in contraction appeared to continue. HTFs produced slightly less contraction than RTFs, but all fibroblast-seeded constructs behaved similarly. All acellular control constructs showed no contraction of the fibrin gel. Histological assessment of the basic tendon analogue demonstrates cellular distribution both within and around the fibrin hydrogel (Figure 4b,c) at a period of 4 weeks in culture. Cellular alignment and collagen production are also observed in the tendon analogue (Figure 4d) as expected from previous studies (Paxton et al., 2012).

Both HObs and RObs could produce a mineralized ECM by day 11–18 when cultured with a mineralizing medium, confirming functional ability (Figure 5). ECM could be discerned as patchy dark granular deposits on a confluent cell monolayer in early culture, which then became the origin of mineralization, and the continued focal point as mineralization progressed. RObs produced a trabecular pattern of mineralized ECM running between the focal nodules, whilst the mineralized ECM of HObs was more diffuse over the whole monolayer with less prominent nodules. Control cultures in maintenance medium produced a similar pattern of ECM formation but with no evidence of alizarin-red positive mineral staining.

3.2 | Three-dimensional co-culture system observations

Curing of the PDMS around the well insert created a 3D replica negative impression culture zone which was transparent for visualization and microscopy of the co-culture construct. The lattice frame component of the overall mould insert successfully allowed simultaneous 6-well preparation and adequately positioned well inserts in all wells without contact with interior well surfaces. PDMS moulded closely to the well insert shape, and the 'tail' impression provided a tight fit for the angled bone anchor and ensured single surface attachment of the tendon analogue onto the intended 'presenting' surface during co-cultures, with no fibrin gel present in the tail area on or around unintended bone anchor surfaces. The 21 mm diameter 'body' impression provided enough space for tendon analogue formation and maturation between the bone and suture anchors, and the freshly polymerized fibrin gel on day 0 crucially covered the entire presenting surface of the bone anchor. The markedly reduced volume of the new culture zone, compared to an original 35 mm diameter well, necessitated a maximum solution volume of approximately 1 mL for fibroblast seeding and medium exchanges after the gel was in place.

ABS printed moulds were faithful to the Tinkercad designs but lacked perfect finish on upper and lower surfaces. This surface roughness translated to a fine notching on the horizontal culture

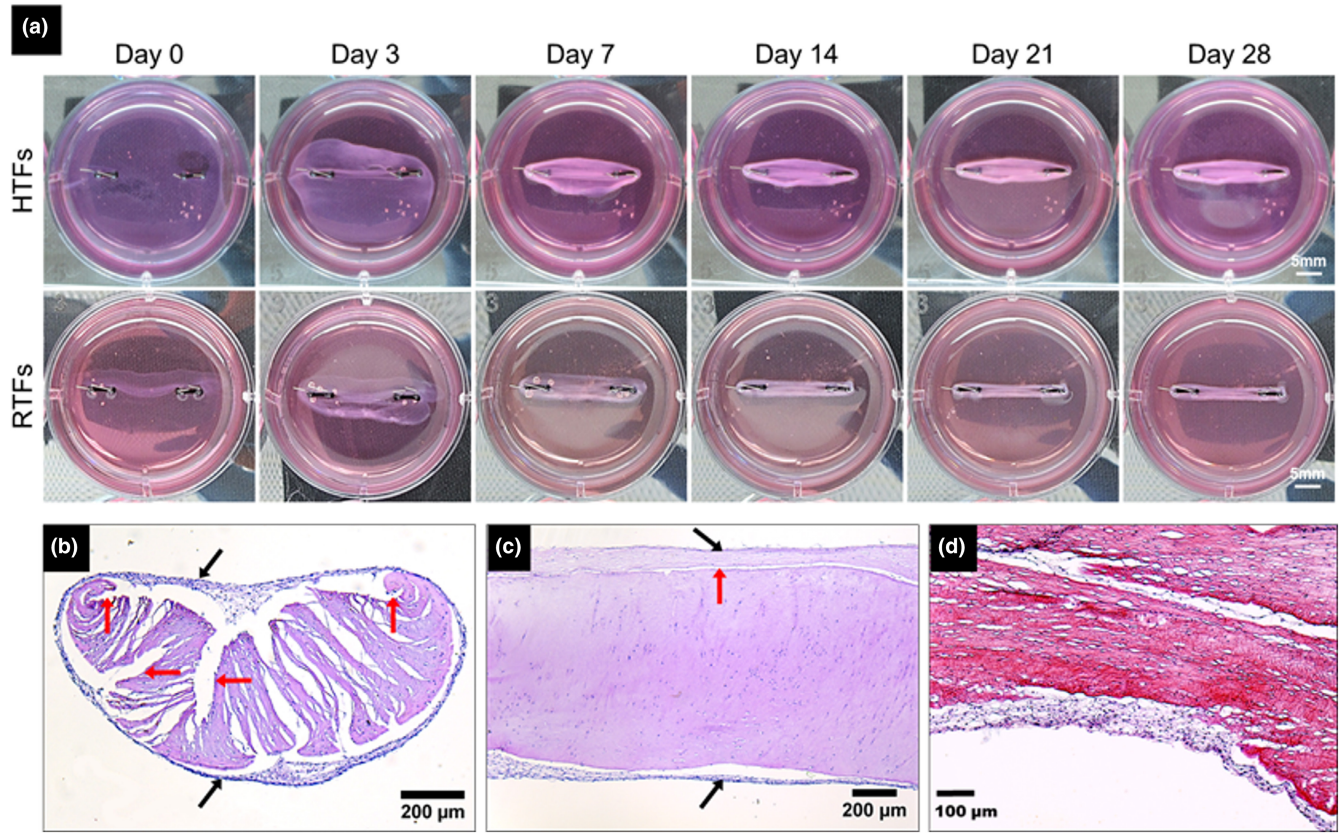

FIGURE 4 Fibroblast and osteoblast functional characterization. (a) Contraction of fibrin gel around suture anchors over time in a basic tendon analogue construct in a 35 mm diameter well, induced by human tendon fibroblasts (HTFs) (*upper panels*) and rat tendon fibroblasts (RTFs) (*lower panels*). Scale bar all wells 5 mm. $n = 3$ in each group; representative images. (b–d) Representative histology micrographs of the tissue-engineered tendon portion of the constructs at 4 weeks in culture with RTFs. (b) Mid-transverse and (c) mid-coronal sections demonstrating cellular fibrin hydrogel in folds (*red arrows*), with a cellular capsular layer (*black arrows*). Haematoxylin and Eosin. (d) Mid-coronal section demonstrating cellular alignment in the axis of tension and collagen (*blue*) produced in the peri-cellular and capsular regions. Masson's Trichrome stain.

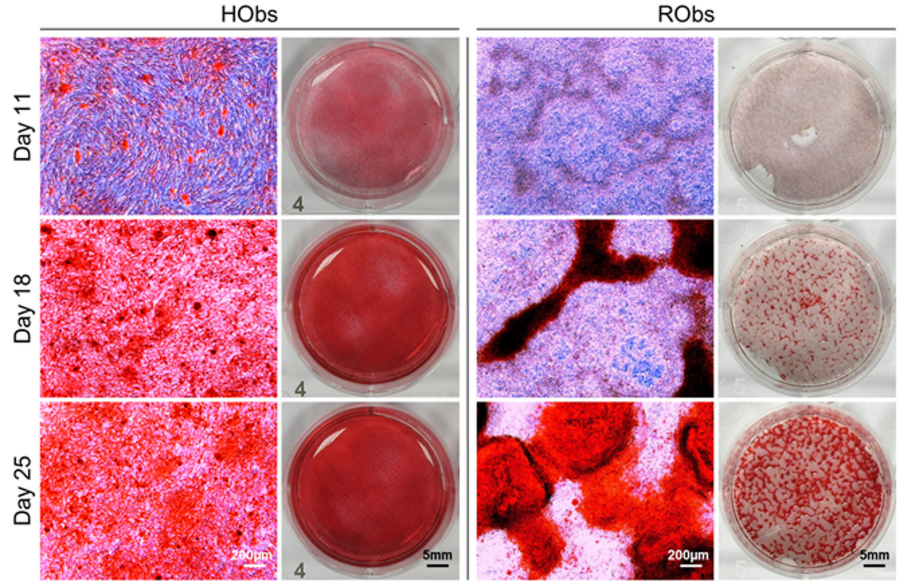

FIGURE 5 Alizarin-red positive extracellular matrix (ECM) mineral staining developing over time on microscopy and overview photography produced by human osteoblasts (HObs) (*left panels*) and rat osteoblasts (RObs) (*right panels*). Red-orange stain indicates calcium presence. Scale bar all micrographs 200 µm, all wells 5 mm. $n = 2$ in each group at each time point; representative images.

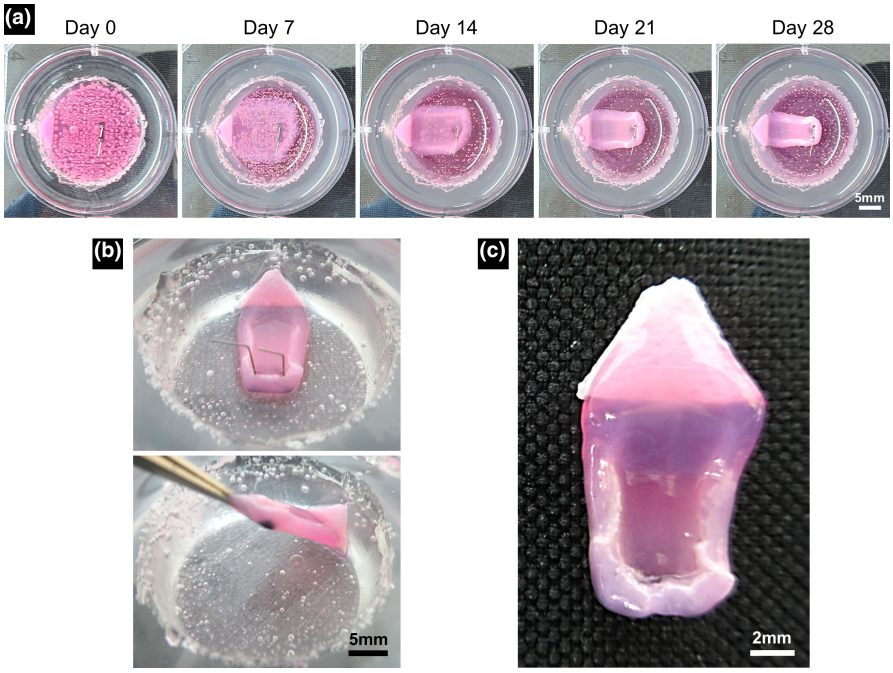

FIGURE 6 'Universal' size human co-culture model system and construct. (a) Representative formation of a tendon–bone construct by human fibroblast-induced fibrin gel contraction over time onto a specifically sized (average) human osteoblast-seeded bone anchor in a 35 mm diameter (original) well. Scale bar all wells 5 mm. $n = 3$. (b) Superior oblique views of the day 28 construct without culture medium, with the suture anchor still pinned in place (*upper panel*) and with gentle axial tension on the tendon analogue with forceps (*lower panel*). Scale bar all wells 5 mm. (c) Overview of the day 28 construct removed from culture.

zone surface, but this did not appear to macroscopically impinge on fibrin gel contraction and did not require any gel release procedures from the under surface. The printed mould surface texturing also resulted in a roughened presenting surface to the bone anchor (see Figure 1), but this was likely advantageous in aiding attachment and integration of the inserting tendon analogue.

Notably, air bubbles became trapped under the surface of the well insert during PDMS curing (see Figures 3d–f, 6 and 7), usually <1 mm diameter but occasionally as larger coalesced bubbles of >5 mm. Although these bubbles lay below the flat culture surface and did not cause undulation of the top surface of the PDMS, removal of the well insert moulds from the cured PDMS did occasionally result in penetration into the larger bubbles, rendering the well unsuitable for use.

3.3 | 'Universal' human tendon–bone co-cultures

The 3D co-culture system was able to direct the attachment of a HTF-contracted fibrin hydrogel tendon analogue onto a single attachment surface of an angled HOb-seeded bone anchor, with a tendon insertion angle and attachment area matched to the average angle and dimensions, respectively, of the adult human FDP attachment (Figure 6). Fibrin gel contraction proceeded comparably over time to the basic tendon analogue constructs forming between 2 suture anchors (see Figure 4a), with the majority of contraction over the first week followed by more minimal progressive contraction beyond day 14 (Figure 6a). However, the co-culture system was able to manipulate the tendon analogue to remain attached to the bone anchor presenting surface whilst it contracted around a single vertically orientated suture that also guided the width of the formed tendon.

The tendon–bone interface remained intact with gentle axial tension (Figure 6b) and during extraction of the day 28 constructs from the 3D co-culture system after cutting through the PDMS (Figure 6c). Axial tension demonstrated that tendon analogue attachment appeared focused towards the lower aspect of the bone anchor presenting surface (Figure 6b); however, in the relaxed extracted state, the tendon–bone interface was displayed over the whole of the bone anchor presenting surface (Figure 6c). The extracted constructs demonstrated a slightly shortened tendon analogue length (Figure 6c) compared to during culture, highlighting the tension provided by the pinned suture anchor in the co-culture system.

3.4 | Multi-size tendon–bone co-cultures

The co-culture system was also able to produce tendon–bone constructs of varying sizes, relating to the previously established 3 size groupings of the adult human FDP insertion (Figure 7). The constructs formed through fibroblast-seeded fibrin gel contraction (Figure 7a) in the same manner as the 'universal' size construct (see Figure 6), but the tendon analogues were guided to attach to a greater or smaller surface area of bony interface, dictated by the size of the 'tail impression' and contained bone anchor. As such,

FIGURE 7 Multi-size co-culture model system and constructs. (a) Representative formation of 'large', 'medium' and 'small' tendon–bone constructs by fibroblast-induced fibrin gel contraction over time onto different size levels of osteoblast-seeded bone anchors in 35 mm diameter (original) wells. Scale bar all wells 5 mm. $n = 3$ for each size. (b) Superior oblique views of the day 28 constructs without culture medium, with the suture anchor still pinned in place (*upper panels*) and with gentle axial tension on the tendon analogue with forceps (*lower panels*). Scale bar all wells 5 mm.

and also relative to the size variation of the suture anchors, the fibrin gel contraction appeared greatest in 'small' sized models, followed by 'medium' and then 'large'. The tendon–bone attachment remained intact in all co-cultures. Gentle axial tension on the formed constructs at day 28 again suggested the focus of tendon analogue attachment over the lower aspect of the bone anchor presenting surface (Figure 7b).

4 | DISCUSSION

This study aimed to demonstrate the integration of real human anatomical morphometrics into a previously established non-anatomical ITE enthesis model. The work served as a proof of concept for the important principle that will enhance the clinical applicability of any future, or previously developed, ITE model. This was accomplished through manipulation of the 3D co-culture environment using a silicone impression negative shape system, which allowed guided attachment of a tendon analogue onto a specifically shaped bone anchor surface area at a precise insertion angle. The model system was successfully trialled with different sizes and cell species, further demonstrating versatility and applicability to ITE models focusing on different body regions or utilizing different cellular approaches.

Morphological features at the enthesis are inherently related to the local biomechanics, as the influence of mechanical factors dictates the principle of 'form follows function' underpinning Wolff's Law (Benjamin et al., 2006; Milz et al., 2005). The tendon enthesis functions to dissipate stress and provide anchorage as it transfers force through the biomechanically distinct structures of tendon to bone; tissues differing in Young's modulus between 200 MPa and 20 GPa, respectively (Thomopoulos et al., 2010). The flared shape as tendons attach to bone provides a greater contact surface area for

attachment and dispersal of interfacial stress forces, and resistance to the effects of insertional angle change during joint movement (Benjamin et al., 2006; Schlecht, 2012), whilst the attachment angle itself affects strain concentration. Regarding the FDP insertion, the previous findings of a consistent shape (trapezoid) and tendon fibre angle (30°) suggests that these are features important to mechanical stability, balancing increased surface area with acceptable stress concentration (Mortimer et al., 2021). The application of these features to an ITE model, as described here, therefore, integrates essential biomechanical characteristics, providing a significant step towards recreating the in vivo environment. It is, therefore, essential that these morphological features should be considered and applied to any ITE model to augment its research utility and potential clinical applicability.

The key morphological features of the FDP enthesis were successfully realized in vitro by applying anatomical analysis of the native insertion to 3D CAD of a moulded well insert (Figure 2), to then create a negative silicone impression that reshapes a standard culture well into a precise housing for 3D co-culture assembly (Figure 3). This is a simple stepwise process of reverse design, which can be applied as an anatomical design method of 3D enthesis models in any anatomical region. The study also demonstrates that this technique is scalable to different 3D dimensions; both as fine-tuning of small, but clinically important, dimensions of the same model, as shown with the 3-level sizes described here (Figure 7), but also with the potential to expand to larger relevant magnitudes. The FDP enthesis provided a suitable size to develop the overall methodological approach in standard 35 mm culture wells of a 6-well plate, but the same methodology is applicable to any in vitro culture accessories for the development of diverse model sizes. With this adaptability, this approach may also be used to generate other ITE models of other common injury sites where bone–tendon/ligament healing is required, such as the ligaments of the ankle (Doherty et al., 2014; Herzog et al., 2019), the anterior cruciate ligament (Bram et al., 2021; Kaeding et al., 2017), the Achilles (calcaneal) tendon (Kvist, 1994; Saltzman & Tearse, 1998) or rotator cuff group (Fitzpatrick et al., 2022; Patel & Amini, 2022). Indeed, the increased need for models to investigate ITE approaches has been highlighted elsewhere (Calejo et al., 2019; Lei et al., 2021; Patel et al., 2018; Sensini et al., 2021), yet our approach is unique as it considers and proposes that anatomical morphometric data should be included in co-culture system design to ensure that anatomical and clinically applicability is at the forefront of ITE design strategy.

Our unique design approach is based upon the ability to accurately fabricate and manipulate the dimensions of cellular scaffolds, as a critical material property in addition to providing a replacement ECM. This study employed the fibrin hydrogel and brushite calcium phosphate salt soft-hard tissue constructs previously designed by Paxton, Grover, and Baar (2010), which has shown promising properties of soft tissue collagen fibre development and soft-hard interface strength (Paxton, Donnelly, et al., 2010) and allowed control of the separate tissue dimensions. Fibrin is classically used to create tendon constructs by contracting around and between anchoring materials under tension (Bayer et al., 2010; Kapacee et al., 2008; Paxton, Wudebwe, et al., 2012), but a key advancement in the adaptation of the previously established model (Paxton, Grover, & Baar, 2010) in this study is the attachment of the fibrin tendon analogue to a single bone anchor surface. This was achieved through the careful design of the integration between the 'tail' and 'body' regions of the well insert, as well as the 'tail' shape and presenting angle (Figures 2 and 3). Axial tension on the tendon analogue demonstrated an intact soft-hard interface, with these model components expected to achieve an interface ultimate tensile strength in the same order of magnitude as embryonic ligaments (Paxton, Grover, & Baar, 2010). Encouragingly, a previous study has also used electron microscopy to demonstrate that the fibrin, and developing replacement collagen fibres, grow into the porous brushite (Paxton, Grover, & Baar, 2010), creating a microscopic interface of interlocking mixed tissues much like the native enthesis. However, it was observed in the current study that the focus of the tendon analogue attachment was on the lower aspect on the bone anchor presenting surface when axial tension was applied. This was likely due to a combination of too little a volume of fibrin hydrogel, over-contraction of the fibrin hydrogel, and gravity. To further refine the current model, an optimum balance of initial fibrin hydrogel volume and fibroblast cell density for controlled contraction and attachment over the entire bone anchor presenting surface requires systematic investigation. Less significant material concerns can also be remedied, such as eliminating the surface roughness of the culture surface by using higher resolution 3D printed thermoplastics or by varying the printing material or technique used (Li et al., 2022; Stansbury & Idacavage, 2016). Also, removing air bubbles from the PDMS by curing under negative pressure vacuum (Luo et al., 2010), or vacuum desiccation, may solve the existing issues with clarity of the PDMS well surround which prevents clear visualization under light microscopy. Most promising would be the application of 3D CAD design and 3D printing to manufacture the cell culture moulds directly using more novel techniques, enabling printing in softer materials than the thermoplastics presented here (Chen et al., 2020; Li et al., 2022). With these exciting possibilities, the general model premise demonstrated here shows significant potential as a 3D enthesis co-culture model, with improved clinical applicability by this amalgamation with anatomical construction. Furthermore, advances in 3D bioprinting technologies (Gupta & Bit, 2022; Zhang et al., 2021) may bring anatomical design and fabrication to the forefront of model design for enthesis ITE.

Further to this, the versatility, adaptability and scalability of the design concept described here allows integration of the technique into studies with a greater focus on interface development, as the defining feature of ITE. A key extension will be combining anatomically designed models with specially designed bioreactors, where the native anatomical morphology may act synergistically with controlled maturation and resulting gradient properties of

the interface, such as mechanical conditioning and timed biochemical manipulation, to escalate overall functionality. With further studies to inform optimum material and cell components, in addition to vital studies on the nutrient availability and diffusion of these throughout the engineered tissue, the addition of anatomical design may provide a key advancement in creating a native enthesis in vitro.

5 | CONCLUSIONS

This study is the first to demonstrate the application of anatomical morphometrics to ITE model design and is an important development towards replicating the native enthesis. An FDP enthesis co-culture model is described, as pre-analysed morphometric data was available, but provides a template methodological approach that can be scaled to construct ITE models of any anatomical region. ITE provides a vital avenue for therapeutic advances, and basing design upon the original anatomical framework will expedite its clinical translation.

AUTHOR CONTRIBUTIONS

Conceptualization, J.W.M. and J.Z.P.; *methodology*: J.W.M. and J.Z.P.; *software*: J.W.M.; *validation*, J.W.M., P.A.R. and J.Z.P.; *formal analysis*, J.W.M. and J.Z.P.; *investigation*, J.W.M.; *resources*, P.A.R. and J.Z.P.; *data curation*, J.W.M. and J.Z.P.; *writing – original draft preparation*, J.W.M. and J.Z.P.; *writing – review and editing*, J.W.M., P.A.R. and J.Z.P.; *visualization*, J.W.M. and J.Z.P.; *supervision*, P.A.R. and J.Z.P.; *project administration*, P.A.R. and J.Z.P.; *funding acquisition*, P.A.R. and J.Z.P. All authors have read and agreed to the published version of the manuscript.

ACKNOWLEDGMENTS

The authors would like to thank the patients who voluntarily consented to providing their discard surgical tissue for the establishment of human fibroblast and osteoblast cell lines; Miriam Graute for the initial concept of a well insert and lattice frame mould design; and Richard Collins and Gosia Walton at the Edinburgh College of Art for 3D printing the moulds.

FUNDING INFORMATION

This research was funded by Orthopaedic Research UK, grant number 528 and The Rooney Plastic Surgery and Reconstructive Surgery Trust ('The Rooney').

DATA AVAILABILITY STATEMENT

The data that support the findings of this study are available from the corresponding author upon reasonable request.

ORCID

Jeremy W. Mortimer https://orcid.org/0000-0002-8727-8392
Jennifer Z. Paxton https://orcid.org/0000-0002-6061-8051

REFERENCES

Abergo, M.O. & Shamrock, A.G. (2022) Jersey finger. In: *StatPearls [Internet]*. Treasure Island (FL): StatPearls Publishing.

Antoni, D., Burckel, H., Josset, E. & Noel, G. (2015) Three-dimensional cell culture: a breakthrough in vivo. *IJMS*, 16, 5517–5527. Available from: https://doi.org/10.3390/ijms16035517

Apostolakos, J., Durant, T.J., Dwyer, C.R., Russell, R.P., Weinreb, J.H., Alaee, F. et al. (2014) The enthesis: a review of the tendon-to-bone insertion. *Muscles, Ligaments and Tendons Journal*, 4, 333–342.

Bachoura, A., Ferikes, A.J. & Lubahn, J.D. (2017) A review of mallet finger and jersey finger injuries in the athlete. *Current Reviews in Musculoskeletal Medicine*, 10, 1–9. Available from: https://doi.org/10.1007/s12178-017-9395-6

Bakker, A.D. & Klein-Nulend, J. (2012) Osteoblast isolation from murine calvaria and long bones. In: Helfrich, M.H. & Ralston, S.H. (Eds.) *Bone research protocols, methods in molecular biology*. Totowa, NJ: Humana Press, pp. 19–29. Available from: https://doi.org/10.1007/978-1-61779-415-5_2

Bayer, M.L., Yeung, C.-Y.C., Kadler, K.E., Qvortrup, K., Baar, K., Svensson, R.B. et al. (2010) The initiation of embryonic-like collagen fibrillogenesis by adult human tendon fibroblasts when cultured under tension. *Biomaterials*, 31, 4889–4897. Available from: https://doi.org/10.1016/j.biomaterials.2010.02.062

Benjamin, M., Evans, E.J., Rao, R.D., Findlay, J.A. & Pemberton, D.J. (1991) Quantitative differences in the histology of the attachment zones of the meniscal horns in the knee joint of man. *Journal of Anatomy*, 177, 127–134.

Benjamin, M. & Ralphs, J.R. (1998) Fibrocartilage in tendons and ligaments—an adaptation to compressive load. *Journal of Anatomy*, 193, 481–494. Available from: https://doi.org/10.1046/j.1469-7580.1998.19340481.x

Benjamin, M., Toumi, H., Ralphs, J.R., Bydder, G., Best, T.M. & Milz, S. (2006) Where tendons and ligaments meet bone: attachment sites ('entheses') in relation to exercise and/or mechanical load. *Journal of Anatomy*, 208, 471–490. Available from: https://doi.org/10.1111/j.1469-7580.2006.00540.x

Bicho, D., Pina, S., Oliveira, J.M. & Reis, R.L. (2018) In vitro mimetic models for the bone-cartilage interface regeneration. In: Oliveira, J.M., Pina, S., Reis, R.L. & San Roman, J. (Eds.) *Osteochondral tissue engineering*. Cham: Springer International Publishing, pp. 373–394. Available from: https://doi.org/10.1007/978-3-319-76735-2_17

Boys, A.J., McCorry, M.C., Rodeo, S., Bonassar, L.J. & Estroff, L.A. (2017) Next generation tissue engineering of orthopedic soft tissue-to-bone interfaces. *MRS Communications*, 7, 289–308. Available from: https://doi.org/10.1557/mrc.2017.91

Bram, J.T., Magee, L.C., Mehta, N.N., Patel, N.M. & Ganley, T.J. (2021) Anterior cruciate ligament injury incidence in adolescent athletes: a systematic review and meta-analysis. *The American Journal of Sports Medicine*, 49, 1962–1972. Available from: https://doi.org/10.1177/0363546520959619

Calejo, I., Costa-Almeida, R., Reis, R.L. & Gomes, M.E. (2019) Enthesis tissue engineering: biological requirements meet at the interface. *Tissue Engineering Part B: Reviews*, 25, 330–356. Available from: https://doi.org/10.1089/ten.teb.2018.0383

Chen, S., Tan, W.S., Bin Juhari, M.A., Shi, Q., Cheng, X.S., Chan, W.L. et al. (2020) Freeform 3D printing of soft matters: recent advances in technology for biomedical engineering. *Biomedical Engineering Letters*, 10, 453–479. Available from: https://doi.org/10.1007/s13534-020-00171-8

de Putter, C.E., Selles, R.W., Polinder, S., Panneman, M.J.M., Hovius, S.E.R. & van Beeck, E.F. (2012) Economic impact of hand and wrist injuries: health-care costs and productivity costs in a population-based study. *Journal of Bone and Joint Surgery*, 94, e56. Available from: https://doi.org/10.2106/JBJS.K.00561

Doherty, C., Delahunt, E., Caulfield, B., Hertel, J., Ryan, J. & Bleakley, C. (2014) The incidence and prevalence of ankle sprain injury: a systematic review and meta-analysis of prospective epidemiological studies. *Sports Medicine*, 44, 123–140. Available from: https://doi.org/10.1007/s40279-013-0102-5

Doschak, M.R. & Zernicke, R.F. (2005) Structure, function and adaptation of bone–tendon and bone–ligament complexes. *Journal of Musculoskeletal & Neuronal Interactions*, 5, 35–40.

Evans, E.J., Benjamin, M. & Pemberton, D.J. (1990) Fibrocartilage in the attachment zones of the quadriceps tendon and patellar ligament of man. *Journal of Anatomy*, 171, 155–162.

Fitzpatrick, L.A., Atinga, A., White, L., Henry, P.D.G. & Probyn, L. (2022) Rotator cuff injury and repair. *Seminars in Musculoskeletal Radiology*, 26, 585–596. Available from: https://doi.org/10.1055/s-0042-1756167

Font Tellado, S., Balmayor, E.R. & van Griensven, M. (2015) Strategies to engineer tendon/ligament-to-bone interface: biomaterials, cells and growth factors. *Advanced Drug Delivery Reviews*, 94, 126–140. Available from: https://doi.org/10.1016/j.addr.2015.03.004

Galatz, L.M., Sandell, L.J., Rothermich, S.Y., Das, R., Mastny, A., Havlioglu, N. et al. (2006) Characteristics of the rat supraspinatus tendon during tendon-to-bone healing after acute injury. *Journal of Orthopaedic Research*, 24, 541–550. Available from: https://doi.org/10.1002/jor.20067

Goers, L., Freemont, P. & Polizzi, K.M. (2014) Co-culture systems and technologies: taking synthetic biology to the next level. *Journal of the Royal Society Interface*, 11, 20140065. Available from: https://doi.org/10.1098/rsif.2014.0065

Gupta, S. & Bit, A. (2022) 3D bioprinting in tissue engineering and regenerative medicine. *Cell and Tissue Banking*, 23, 199–212. Available from: https://doi.org/10.1007/s10561-021-09936-6

Herzog, M.M., Kerr, Z.Y., Marshall, S.W. & Wikstrom, E.A. (2019) Epidemiology of ankle sprains and chronic ankle instability. *Journal of Athletic Training*, 54, 603–610. Available from: https://doi.org/10.4085/1062-6050-447-17

Huq, S., George, S. & Boyce, D.E. (2013) Zone 1 flexor tendon injuries: a review of the current treatment options for acute injuries. *Journal of Plastic, Reconstructive & Aesthetic Surgery*, 66, 1023–1031. Available from: https://doi.org/10.1016/j.bjps.2013.04.026

Kaeding, C.C., Léger-St-Jean, B. & Magnussen, R.A. (2017) Epidemiology and diagnosis of anterior cruciate ligament injuries. *Clinics in Sports Medicine*, 36, 1–8. Available from: https://doi.org/10.1016/j.csm.2016.08.001

Kapacee, Z., Richardson, S., Lu, Y., Starborg, T., Holmes, D., Baar, K. et al. (2008) Tension is required for fibripositor formation. *Matrix Biology*, 27, 371–375. Available from: https://doi.org/10.1016/j.matbio.2007.11.006

Kvist, M. (1994) Achilles tendon injuries in athletes. *Sports Medicine*, 18, 173–201. Available from: https://doi.org/10.2165/00007256-199418030-00004

Leddy, J.P. & Packer, J.W. (1977) Avulsion of the profundus tendon insertion in athletes. *The Journal of Hand Surgery*, 2, 66–69. Available from: https://doi.org/10.1016/S0363-5023(77)80012-9

Lei, T., Zhang, T., Ju, W., Chen, X., Heng, B.C., Shen, W. et al. (2021) Biomimetic strategies for tendon/ligament-to-bone interface regeneration. *Bioactive Materials*, 6, 2491–2510. Available from: https://doi.org/10.1016/j.bioactmat.2021.01.022

Li, B., Zhang, M., Lu, Q., Zhang, B., Miao, Z., Li, L. et al. (2022) Application and development of modern 3D printing technology in the field of orthopedics. *BioMed Research International*, 2022, 1–15. Available from: https://doi.org/10.1155/2022/8759060

Liu, S.H., Panossian, V., Al-Shaikh, R., Tomin, E., Shepherd, E., Finerman, G.A. et al. (1997) Morphology and matrix composition during early tendon to bone healing. *Clinical Orthopaedics and Related Research*, 339, 253–260. Available from: https://doi.org/10.1097/00003086-199706000-00034

Loukopoulou, C., Mortimer, J. & Paxton, J. (2022) Making connections: using anatomy to guide tissue engineering approaches at the enthesis. *eCells and Materials Journal (eCM)*, 43, 179–201. Available from: https://doi.org/10.22203/eCM.v043a14

Luo, C., Ni, X., Liu, L., Nomura, S.M. & Chen, Y. (2010) Degassing-assisted patterning of cell culture surfaces. *Biotechnology and Bioengineering*, 105, 854–859. Available from: https://doi.org/10.1002/bit.22586

Milz, S., Benjamin, M. & Putz, R. (2005) Molecular parameters indicating adaptation to mechanical stress in fibrous connective tissue. *Advances in Anatomy, Embryology, and Cell Biology*, 178, 1–71.

Milz, S., Rufai, A., Buettner, A., Putz, R., Ralphs, J.R. & Benjamin, M. (2002) Three-dimensional reconstructions of the Achilles tendon insertion in man. *Journal of Anatomy*, 200, 145–152. Available from: https://doi.org/10.1046/j.0021-8782.2001.00016.x

Moffat, K.L., Wang, I.-N.E., Rodeo, S.A. & Lu, H.H. (2009) Orthopedic interface tissue engineering for the biological fixation of soft tissue grafts. *Clinics in Sports Medicine*, 28, 157–176. Available from: https://doi.org/10.1016/j.csm.2008.08.006

Moiemen, N.S. & Elliot, D. (2000) Primary flexor tendon repair in zone 1. *Journal of Hand Surgery*, 25, 78–84. Available from: https://doi.org/10.1054/jhsb.1999.0319

Mortimer, J.W., Alsaykhan, H., Vadibeler, S., Rust, P.A. & Paxton, J.Z. (2021) Anatomy and histomorphology of the flexor digitorum profundus enthesis: functional implications for tissue engineering and surgery. *BMC Musculoskeletal Disorders*, 22, 1032. Available from: https://doi.org/10.1186/s12891-021-04922-1

Patel, M. & Amini, M.H. (2022) Management of acute rotator cuff tears. *Orthopedic Clinics of North America*, 53, 69–76. Available from: https://doi.org/10.1016/j.ocl.2021.08.003

Patel, S., Caldwell, J., Doty, S.B., Levine, W.N., Rodeo, S., Soslowsky, L.J. et al. (2018) Integrating soft and hard tissues via interface tissue engineering. *Journal of Orthopaedic Research*, 36, 1069–1077. Available from: https://doi.org/10.1002/jor.23810

Paxton, J., Baar, K. & Grover, L. (2012) Current progress in enthesis repair: strategies for interfacial tissue engineering. *Orthopaedic and Muscular System*, S1, 003. Available from: https://doi.org/10.4172/2161-0533.s1-003

Paxton, J.Z., Donnelly, K., Keatch, R.P. & Baar, K. (2009) Engineering the bone–ligament interface using polyethylene glycol diacrylate incorporated with hydroxyapatite. *Tissue Engineering Part A*, 15, 1201–1209. Available from: https://doi.org/10.1089/ten.tea.2008.0105

Paxton, J.Z., Donnelly, K., Keatch, R.P., Baar, K. & Grover, L.M. (2010) Factors affecting the longevity and strength in an in vitro model of the bone–ligament interface. *Annals of Biomedical Engineering*, 38, 2155–2166. Available from: https://doi.org/10.1007/s10439-010-0044-0

Paxton, J.Z., Grover, L.M. & Baar, K. (2010) Engineering an in vitro model of a functional ligament from bone to bone. *Tissue Engineering Part A*, 16, 3515–3525. Available from: https://doi.org/10.1089/ten.tea.2010.0039

Paxton, J.Z., Wudebwe, U.N.G., Wang, A., Woods, D. & Grover, L.M. (2012) Monitoring sinew contraction during formation of tissue-engineered fibrin-based ligament constructs. *Tissue Engineering Part A*, 18, 1596–1607. Available from: https://doi.org/10.1089/ten.tea.2011.0535

Rodeo, S.A., Arnoczky, S.P., Torzilli, P.A., Hidaka, C. & Warren, R.F. (1993) Tendon-healing in a bone tunnel. A biomechanical and histological study in the dog. *The Journal of Bone & Joint Surgery*, 75, 1795–1803. Available from: https://doi.org/10.2106/00004623-199312000-00009

Ruchelsman, D.E., Christoforou, D., Wasserman, B., Lee, S.K. & Rettig, M.E. (2011) Avulsion injuries of the flexor digitorum profundus tendon. *Journal of the American Academy of Orthopaedic Surgeons*, 19, 152–162. Available from: https://doi.org/10.5435/00124635-201103000-00004

Saltzman, C.L. & Tearse, D.S. (1998) Achilles tendon injuries. *Journal of the American Academy of Orthopaedic Surgeons*, 6, 316–325. Available from: https://doi.org/10.5435/00124635-199809000-00007

Schlecht, S.H. (2012) Understanding entheses: bridging the gap between clinical and anthropological perspectives. *The Anatomical Record*, 295, 1239–1251. Available from: https://doi.org/10.1002/ar.22516

Sensini, A., Massafra, G., Gotti, C., Zucchelli, A. & Cristofolini, L. (2021) Tissue engineering for the insertions of tendons and ligaments: an overview of electrospun biomaterials and structures. *Frontiers in Bioengineering and Biotechnology*, 9, 645544. Available from: https://doi.org/10.3389/fbioe.2021.645544

Shapiro, L.M. & Kamal, R.N. (2020) Evaluation and treatment of flexor tendon and pulley injuries in athletes. *Clinics in Sports Medicine*, 39, 279–297. Available from: https://doi.org/10.1016/j.csm.2019.12.004

Shaw, H.M. & Benjamin, M. (2007) Structure–function relationships of entheses in relation to mechanical load and exercise: tendon and ligament entheses. *Scandinavian Journal of Medicine & Science in Sports*, 17, 303–315. Available from: https://doi.org/10.1111/j.1600-0838.2007.00689.x

Shiroud Heidari, B., Ruan, R., De-Juan-Pardo, E.M., Zheng, M. & Doyle, B. (2021) Biofabrication and signaling strategies for tendon/ligament interfacial tissue engineering. *ACS Biomaterials Science & Engineering*, 7, 383–399. Available from: https://doi.org/10.1021/acsbiomaterials.0c00731

Silva, M.J., Boyer, M.I., Ditsios, K., Burns, M.E., Harwood, F.L., Amiel, D. et al. (2002) The insertion site of the canine flexor digitorum profundus tendon heals slowly following injury and suture repair. *Journal of Orthopaedic Research*, 20, 447–453. Available from: https://doi.org/10.1016/S0736-0266(01)00139-5

Silva, M.J., Thomopoulos, S., Kusano, N., Zaegel, M.A., Harwood, F.L., Matsuzaki, H. et al. (2006) Early healing of flexor tendon insertion site injuries: tunnel repair is mechanically and histologically inferior to surface repair in a canine model. *Journal of Orthopaedic Research*, 24, 990–1000. Available from: https://doi.org/10.1002/jor.20084

Smith, L., Xia, Y., Galatz, L.M., Genin, G.M. & Thomopoulos, S. (2012) Tissue-engineering strategies for the tendon/ligament-to-bone insertion. *Connective Tissue Research*, 53, 95–105. Available from: https://doi.org/10.3109/03008207.2011.650804

Stansbury, J.W. & Idacavage, M.J. (2016) 3D printing with polymers: challenges among expanding options and opportunities. *Dental Materials*, 32, 54–64. Available from: https://doi.org/10.1016/j.dental.2015.09.018

Tempelaere, C., Brun, M., Doursounian, L. & Feron, J.-M. (2017) Traumatic avulsion of the flexor digitorum profundus tendon. Jersey finger, a 29 cases report. *Hand Surgery and Rehabilitation*, 36, 368–372. Available from: https://doi.org/10.1016/j.hansur.2017.06.002

Thomopoulos, S., Genin, G.M. & Galatz, L.M. (2010) The development and morphogenesis of the tendon-to-bone insertion—what development can teach us about healing. *Journal of Musculoskeletal & Neuronal Interactions*, 10, 35–45.

Thomopoulos, S., Williams, G.R. & Soslowsky, L.J. (2003) Tendon to bone healing: differences in biomechanical, structural, and compositional properties due to a range of activity levels. *Journal of Biomechanical Engineering*, 125, 106–113. Available from: https://doi.org/10.1115/1.1536660

Tuttle, H.G., Olvey, S.P. & Stern, P.J. (2006) Tendon avulsion injuries of the distal phalanx. *Clinical Orthopaedics and Related Research*, 445, 157–168. Available from: https://doi.org/10.1097/01.blo.0000205903.51727.62

Wang, I.-N.E., Shan, J., Choi, R., Oh, S., Kepler, C.K., Chen, F.H. et al. (2007) Role of osteoblast–fibroblast interactions in the formation of the ligament-to-bone interface. *Journal of Orthopaedic Research*, 25, 1609–1620. Available from: https://doi.org/10.1002/jor.20475

Yang, P.J. & Temenoff, J.S. (2009) Engineering orthopedic tissue interfaces. *Tissue Engineering Part B: Reviews*, 15, 127–141. Available from: https://doi.org/10.1089/ten.teb.2008.0371

Zhang, J., Wehrle, E., Rubert, M. & Müller, R. (2021) 3D bioprinting of human tissues: biofabrication, bioinks, and bioreactors. *IJMS*, 22, 3971. Available from: https://doi.org/10.3390/ijms22083971

Zhang, X., Shao, X. & Zhang, K. (2014) Pull-out wire traction for the treatment of avulsion of the flexor digitorum profundus from its insertion. *The Journal of Hand Surgery, European Volume*, 39, 667–669. Available from: https://doi.org/10.1177/1753193412453418

How to cite this article: Mortimer, J.W., Rust, P.A. & Paxton, J.Z. (2024) Anatomical design and production of a novel three-dimensional co-culture system replicating the human flexor digitorum profundus enthesis. *Journal of Anatomy*, 00, 1–14. Available from: https://doi.org/10.1111/joa.14027